Characterizing the n→π* interaction of pyridine with small ketones: a rotational study of pyridine acetone and pyridine 2-butanone

Juan Carlos López, Ibon Alkorta, Alberto Macario, Susana Blanco

▶ **To cite this version:**

HAL Id: hal-03725310

https://univ-rennes.hal.science/hal-03725310

Submitted on 1 Aug 2022

ARTICLE

Characterizing the $n\to\pi^*$ interaction of pyridine with small ketones: a rotational study of pyridine···acetone and pyridine···2-butanone

Juan Carlos López,*[a] Ibon Alkorta [b] Alberto Macario [a†] and Susana Blanco [a]

The complexes formed by pyridine and small ketones as acetone and 2-butanone have been generated in a supersonic jet and characterized by broadband Fourier transform microwave spectroscopy combined with high-level theoretical computations. The spectra of the complexes show the quadrupole coupling hyperfine structure due to the presence of a nitrogen atom and the splittings owing to the low barriers of the internal rotation of the methyl groups bonded to the carbonyl group. The corresponding barriers have been determined from the analysis of the spectra. We show in both complexes, pyridine close a cycle with the ketone carbonyl group through an N···C=O $n\to\pi^*$ tetrel interaction and a C-H···O contact. The $n\to\pi^*$ tetrel bond involves the pyridine N atom lone pair and the ketone carbonyl group with a geometry approaching the Bürgi-Dunitz trajectory for the nucleophilic attack to a carbonyl group.

Introduction

Non-covalent interactions (NCIs) determine the structure and properties of molecules, clusters, or materials, and are central forces in supramolecular chemistry[1,2] and biochemistry. While their study in biological systems is difficult due to the existence of interaction networks and the presence of water molecules, isolated molecular complexes are the best source of information to size the different types of interactions.[3–6] Hydrogen bonding (HB), the best-known NCI, is of fundamental importance in both chemistry and biology. Halogen bonding [7,8] constitutes another type of NCI that has attracted the interest of researchers in the last decades. Other groups of weak NCIs[9] include those called tetrel bonds,[10–12] pnictogen bonds,[13–15] and chalcogen bonds,[16–18] which were known a long time ago but have received those names only very recently.[19,20] It is accepted that these NCIs arise mainly from the interaction of an electrophilic region associated with an atom,[21] identified with hydrogen (hydrogen bond), halogens (halogen bond), or an element of the group 14 (tetrel bond), 15 (pnictogen bond), or 16 (chalcogen bond), with a nucleophilic region, non-bonding or π-bonding electron pairs located in another or the same molecule.[19]

Within this perspective, the so-called $n\to\pi^{*}$[22,23] interactions where the electrophilic region is associated with the carbon atom of carbonyl compounds can be identified as tetrel bonds. $n\to\pi^*$ interactions are structure-determinant in small biomolecules[24–28] and proteins[29,30] but despite their interest, only a few rotational spectroscopy studies have shown these interactions to occur in molecular complexes.[31–34] In their pioneering works from crystal structure survey analysis, Bürgi and Dunitz[35–37] identified those interactions as the experimental basis to map the reaction coordinate for the addition of a nucleophile to a carbonyl group. At large distances, the interaction would occur orthogonally between local dipoles of the nucleophile and the carbonyl group, giving rise to the classification of these NCIs as orthogonal multipolar interactions.[23] However, at short distances the carbonyl group appears to adopt a pyramidal shape, indicating that for close contacts, orbital overlap becomes important.[22,35,38,39] This overlap involves the delocalization of a lone pair (n) of the nucleophile donor group into the antibonding (π^*) orbital of the carbonyl group, so these contacts are called $n\to\pi^*$ interactions.[22] The most important signatures reported for these interactions are: (i) a short contact between the donor atom and the acceptor carbonyl carbon atom, allowing for orbital overlap; (ii) the location of the donor atom along the Bürgi-Dunitz[35] trajectory which maximizes $n\to\pi^*$ orbital overlap; (iii) pyramidalization of the acceptor carbonyl group (see Figure 1).

Rotational spectroscopy studies have shown that $n\to\pi^*$ interactions take place in small biomolecules. For example, they stabilize the most stable conformers of the neurotransmitter GABA[24] or 4(S)-hydroxyproline,[25] and have been observed in β-alanine,[26] 5-aminovaleric acid[27] or aspirin.[28,40] The $n\to\pi^*$ interactions between water and the carbonyl group have also been shown to cooperate with the medium and weak HBs to stabilize the microsolvated adducts of β-propiolactone[34] and benzophenone.[41] Recently the competition between HB and

a. Departamento de Química Física y Química Inorgánica, Facultad de Ciencias, IU CINQUIMA,Universidad de Valladolid, 47011 Valladolid (Spain), susana.blanco@uva.es (S.B.)

b. Instituto de Química Médica (CSIC), Juan de la Cierva 3, 28006 Madrid (Spain); ibon@iqm.csic.es

† Current Address: Département de Physique Moléculaire, IPR (Institut de Physique de Rennes), CNRS-UMR 6251, Université de Rennes 1, F-35000 Rennes, France; alberto.macario@univ-rennes1.fr.

*Correspondence: juancarlos.lopeza@uva.es.

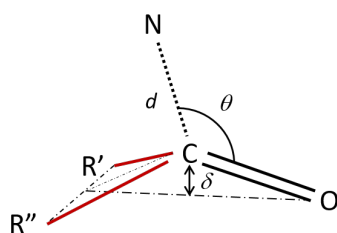$n{\rightarrow}\pi^*$ tetrel interactions has been studied in the complex 3-oxetanone···formaldehyde.[33]

Figure 1. Geometrical parameters associated to the Bürgi-Dunitz trajectory for the addition of a nucleophile, N, to a carbonyl carbon atom.

Pyridine (PY) or its derivatives can be used as nucleophilic catalysts in acylation reactions[42] so the structures of pre-reactive intermediates of PY with carbonyl compounds can be expected to be located along the Bürgi-Dunitz trajectory for nucleophilic addition to the carbonyl group. The complexes of PY with the two smaller carbonyl derivatives formaldehyde (FA)[31] and acetaldehyde (AC)[32] have been already been described and show the signatures of the $n{\rightarrow}\pi^*$ interactions. In both cases, the observed complex presents an $n{\rightarrow}\pi^*$ tetrel bond and a weak CH···O HB. The adduct PY···FA[31] was the first observed complex in the gas phase for which the $n{\rightarrow}\pi^*$ is the main intermolecular interaction. For the PY···AC[32] complex, it was observed that the AC methyl group internal rotation induces a phase-locked intermolecular oscillation along the Bürgi-Dunitz coordinate. The delicate equilibrium between weak attractive and repulsive interactions leads the internal rotation of the AC methyl group to modulate the $n{\rightarrow}\pi^*$ interaction coordinate. This sort of molecular balance extracts energy from the intermolecular interaction to reduce the size of the internal rotation barrier so this tetrel bond can be considered as a sort of supramolecular dynamics catalyst as observed for halogen bonds.[43] In this paper, we present a combined theoretical and rotational study of the complexes of PY with the simplest ketones, acetone (ACE) and 2-butanone (2BU), in order to see if the $n{\rightarrow}\pi^*$ interaction observed for the simplest aldehydes prevails in larger size systems where steric forces may contribute to force the geometry of the adducts to be out of the limiting values predicted for the Bürgi-Dunitz geometry. This would allow us to analyze the consequences of the increasing size of the carbonyl compounds on the strength of the intermolecular interactions. A comparison of the experimental and theoretical data of the four complexes of PY with FA, AC, ACE, and 2BU would shed additional light on modelling the N···C=O $n{\rightarrow}\pi^*$ tetrel bond in systems of different size. Both ketones used here have two methyl tops. These are equivalents in the case of ACE with low barrier values of 266 cm^{-1} as determined from rotational data that would rise to complex splitting patterns in the rotational spectrum.[44] For 2BU only the *trans*-form has been observed[45] and the methyl groups present very different internal rotation barriers, 181.5 cm^{-1} and 763.9 cm^{-1}.[46] It would be interesting to detect if the formation of the PY···ACE and PY···2BU complexes affects the methyl group internal rotational barrier of ACE and 2BU.

Methods

Experimental

Commercial samples of PY, ACE, and 2BU were used without further purification. The spectrum was recorded in the frequency range 2-8 GHz, using a chirped-pulse Fourier transform microwave spectrometer (CP-FTMW)[47] described elsewhere.[48] The supersonic jet was generated by expansion of Ne at backing pressures of about 2 bar through a 0.8 mm diameter pulsed heatable nozzle with molecular pulses of 700 µs duration. PY was located in a reservoir located at the heatable nozzle and ACE, or 2BU, was placed in a reservoir inserted in the gas line just before the nozzle. The spectra were recorded in steps of 2 GHz. Chirp pulses of 4 µs were created by an arbitrary waveform generator and amplified. The polarization signal was radiated from a horn antenna in a direction perpendicular to that of the expanding gas. A molecular transient emission spanning 40 µs is then detected through a second horn antenna, recorded with a digital oscilloscope and Fourier-transformed to the frequency domain. The accuracy of frequency measurements is estimated to be better than 10 kHz, but given the signal-to-noise ratio of some of the observed lines in the fits, these were given estimated measurement errors of 15 kHz except for overlapped lines for which it increased to 30 kHz. Measurements of the spectra were done using the AABS package[49] available as well as many other useful applications on the PROSPE website.[50]

Computational

The potential energy surfaces of the PY···ACE and PY···2BU complexes have been explored with metadynamics sampling in the Crest program.[51] These geometries have been used as a starting point in the optimization at B3LYP[52,53]/6-311++G(2d,p)[54] with the D3BJ[55] empirical dispersion parameters. Further optimizations have been carried out at the MP2[56]/6-311++G(2d,p) level after removing the repeated geometries. Frequency calculations have been carried out at B3LYP and MP2 levels to confirm that the structures obtained correspond to energetic minima. The rotational barrier of the methyl groups was obtained at MP2/6-311++G(2d,p) level by optimization of the TS structures which were confirmed by frequency calculations. The B3LYP and MP2 calculations have been performed with the Gaussian-16[57] program. Although the results obtained at these commonly used levels are enough to assign the rotational spectra, in previous papers[31,32] it has been shown that the experimental $n{\rightarrow}\pi^*$ Bürgi-Dunitz parameters are not well reproduced at those theoretical levels. In those cases, CCSD/6-311++G(2d,p) calculations lead to angles and distances that better reproduce the experimental data. In this work, we have only measured the parent species so to have more accurate structural data, especially to analyze methyl group internal rotation, the two most stable minima of each complex have been reoptimized at CCSD/6-311++G(2d,p). The obtained geometries have been used to evaluate the energy at CCSD(T)/6-311++G(2d,p) including the BSSE correction[58] with the Molpro-2012[59] program. The nuclear quadrupole coupling constants have been calculated at CCSD/6-311++G(2d,p) level

with the Gaussian-16 program. The electrostatic characteristics of the isolated compounds have been characterized using the CCSD wave function generated with the Gaussian-16, analyzed with the Multiwfn program,[60] and plotted with Jmol.[61] The components of the interaction energy have been analyzed with the DFT-SAPT[62] method with the PBE0[63] functional and the aug-cc-pVTZ basis set using the geometries obtained at CCSD level. These calculations have been carried out in the Molpro-2012 program. The electron density of the complexes has been studied using the QTAIM methodology[64] with the AIMAll[65]
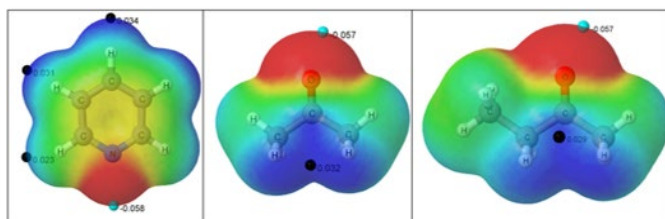

Figure 2. Molecular electrostatic potential on the 0.001 au electron density isosurface. Red and blue colors indicate values > 0.03 au and < -0.03, respectively. The location and values of some of the stationary points in au are indicated.

program and the NCIPlot approach.[66] In addition, the charge transfer stabilization between occupied orbitals of one molecule and empty ones of the other has been studied with the NBO methodology.[67]

Results and discussion

Preliminary calculations

The molecular electrostatic potential (MEP) of two molecules can be used to locate the complementary regions that could provide clues about the intermolecular interactions. In the present case, PY shows a region with negative values of the MEP on the 0.001 au electron density isosurface associated with the lone pair of the nitrogen (see Figure 2) while the positive regions are associated with the hydrogen atoms. In the case of the carbonyl compounds, the positive region is also associated with the hydrogen atoms and above/below the carbonyl group carbon atom and the negative one with the oxygen atom.
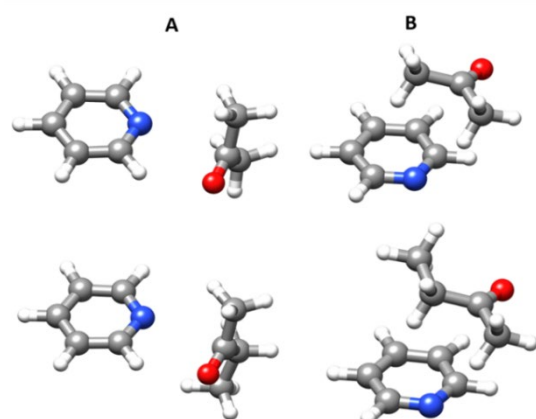

Figure 3. The two most stable forms, labelled as A and B, predicted for pyridine···acetone (upper images) and pyridine···2-butanone (lower images). Forms A in both complexes exhibit a tetrel bond $n \rightarrow \pi^*$ interaction while in B forms the interacting molecules are stacked.

The two most stable conformers found for each adduct, PY···ACE and PY···2BU, are similar (Figure 3) and have been labelled A and B. Conformer A, the most stable form of both complexes, shows a tetrel bond $n \rightarrow \pi^*$ interaction and a weak C=O···H-C contact. In forms B the interacting molecules appear to be stacked. The calculated parameters for the three levels of calculation used are shown in Tables S1-S6.

Rotational spectra

The recorded spectra are dominated by the rotational transitions of the monomers (see Figures S1 and S2). Any complex of PY with ACE or 2BU is expected to show a characteristic quadrupole coupling hyperfine structure (hfs) due to the presence of ^{14}N in PY[68] and the fine structure due to the internal rotation of the methyl tops in ACE[44] or 2BU.[45,46] Although this adds some extra difficulties to the analysis of the spectrum the specific spectral patterns constitute a fingerprint for each rotational transition (see Figures 4 and 5).

The nuclear quadrupole hfs arises from the coupling of the nuclear electric quadrupole moment (eQ) of the ^{14}N atom with the electric field gradient q ($q_{\alpha\beta}=\partial^2V/\partial\alpha\partial\beta$, $\alpha,\beta=a,b,c$) created by the molecular charges at the site of this nucleus. The nuclear spin angular momentum of ^{14}N (I=1) then couples to the overall rotation angular momentum (**J**) to form a resultant **F** (**F=I+J**). The determinable spectroscopic parameters are the elements of the nuclear quadrupole coupling tensor χ, linearly related to the electric field gradient tensor q by χ = eQq. Usually, for ^{14}N, only the diagonal elements of this tensor (χ_{aa}, χ_{bb}, and χ_{cc}) are determined.
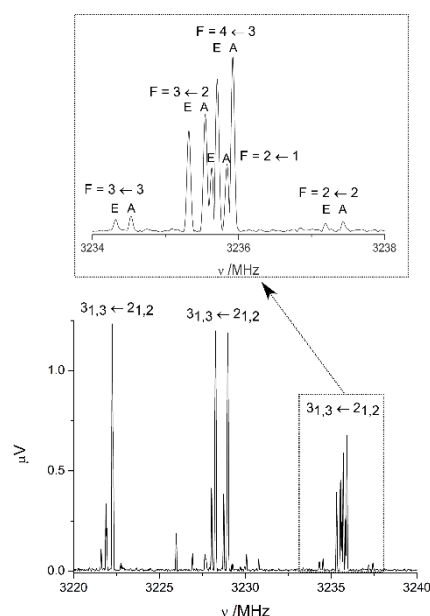
Figure 4. The ^aR-branch J = 3←2 transitions of the complex pyridine···2-butanone. The excerpt shows in detail the $3_{1,2}\leftarrow 2_{1,1}$ transition. The quadrupole coupling components due to the presence of a ^{14}N nucleus in pyridine are labelled with the F quantum number. Each component is further split into the A and E substates due to the coupling between the angular momenta of the overall rotation and the internal rotation of methyl group of 2-butanone bonded to C=O.

For molecules with a single methyl top having a threefold barrier, rotational energy levels split into two torsional

Figure 5. The $4_{0,4} \leftarrow 3_{0,3}$ transition of pyridine···acetone showing the quadrupole coupling structure due to the presence of ^{14}N in pyridine for each of the *AA*, *AE*, *EA* and *EE* substates associated to the internal rotation of the two equivalent methyl groups in acetone subunit.

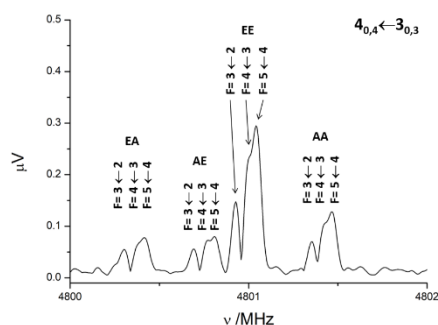sublevels labelled *A* (torsional symmetry σ=0) and the doubly degenerate *E* ($\sigma=\pm1$). In the general case of two equivalent methyl tops,[69] the rotational levels are split into four torsional states labelled *AA*, *AE*, *EA*, and *EE* of 1, 2, 2, and 4-fold degeneracy. The selection rules are such that rotational transitions occur within the torsional substates. These can also be labelled as, (0, 0), ($\pm1,\pm1$), ($\pm1, \mp1$), and [(0,±1) and (±1,0)] using the torsional symmetry label σ and alternatively as *AA* = *A*, *AE* = *E*+, *EA* = *E*−, and *EE* = *G*.[70] For inequivalent tops, the fourfold degenerate state can split into two twofold states or into 3 (*AE* and *EA* not resolved), 4, or 5 (*EE* split).

The assignment of the adducts spectra was based on the computational chemistry predictions for the rotational constants, quadrupole coupling constants, and internal rotation geometrical parameters. The two calculated conformers of each adduct are prolate asymmetric rotors with values of the μ_a electric dipole moment components. In those cases the *J*+1←*J*, ᵃR-branch transitions form groups of lines with characteristic patterns separated at frequency intervals close to the magnitude of the sum of *B* and *C* rotational constants. The initial identification of these transitions allows the complete assignment of the spectra of the most stable forms of both complexes. *a*-, *b*-, and *c*-type spectra were observed for PY···2BU while only *a*- and *b*-type spectra were observed for PY···ACE. The set of observed *J* = 3←2 ᵃR-branch transitions for PY···2BU is shown in Figure 4. In this figure, we can observe in detail the $3_{1,2} \leftarrow 2_{1,1}$ transition split into several components labelled with the *F* quantum number corresponding to the ^{14}N quadrupole coupling hfs. Each hfs component additionally splits into two lines corresponding to the *A* and *E* torsional sublevels attributable to a single methyl top. In Figure 5 the $4_{0,4} \leftarrow 3_{0,3}$ rotational transitions observed for PY···ACE are shown. In this case, apart from the hfs components, each transition is split into four torsional sublevels labelled *AA*, *AE*, *EA*, and *EE* according to the patterns expected for two equivalent methyl tops.

The first analysis of the spectrum of the *A* state of 2BU was done with the CALPGM[71] package using a semirigid rotor Hamiltonian[72] in the S-reduction and Iʳ representation supplemented with quadrupole coupling[73] terms. For the assignments of the *E* state, additional perturbation terms[74] taking into account the deviations of the *E* states from the semirigid rotor behaviour, were included (see Table S7). In a final step, a global fit of the *A* and *E* states was done using XIAM

program[70] which is a version of the internal axis method (IAM) of Woods,[75] and allows us to determine the rotational, centrifugal distortion, quadrupole coupling constants, and several internal rotation parameters including the angles $\angle(i,a)$, $\angle(i,b)$, $\angle(i,c)$, giving the orientation of the top axis relative to the principal inertial axes (see Figure 6). In this fit, the value of the *F* reduced rotational constant for the internal rotation was fixed to the value used for free 2BU[46] using the same program. The determined parameters are given in Table 1 and the observed frequencies are reported in Table S11. No additional *A-E* splittings due to the effects of the second methyl top of 2-BU were observed. The splittings predicted for transitions in the 2-8 GHz range with the barrier value reported for this top in 2-BU monomer fall below the resolution of our spectrometer.

Table 1. Rotational parameters obtained from the internal rotation analysis of the pyridine···2-butanone spectrum and their comparison to those calculated at CCSD/6-311++G(2d,p) level. The centrifugal distortion constants and the V_3 barrier have been calculated at MP2/6-311++G(2d,p).

Param [a]	Obs	Calc
A/MHz	1886.3540(13)[b]	1891.2
B/MHz	540.40505(24)	539.2
C/MHz	535.87635(24)	533.7
D_J/kHz	0.2201(16)	0.18
D_{JK}/kHz	2.247(15)	2.30
D_K/kHz	-0.88(28)	-2.26
d_1/kHz	-0.0050(13)	-0.0046
d_2/kHz	-0.00842(88)	0.0100
χ_{aa}/MHz	-4.0687(20)	-4.47
$(\chi_{bb}-\chi_{cc})$ /MHz	2.2580(38)	1.43
V_3/GHz	6624.85(76)	5927
V_3/cm^{-1}	220.981(26)	197.7
V_3/kJ mol^{-1}	2.59946(30)	2.364
D_{pi2J}/kHz	12.14(59)	
ε/rad	0.6123(35)	0.58
δ/rad	1.609925(72)	1.59
I_α/uÅ^2	[3.1986][c]	3.253
F/GHz	[158.543][c]	155.895
$\angle(i,a)$/°	92.2419(41)	91.2
$\angle(i,b)$/°	54.95(20)	56.6
$\angle(i,c)$/°	35.14(20)	33.4
N	234	
σ/kHz	4.7	

[a] A, B, and C are rotational constants. D_J, D_{JK}, D_K, d_1, and d_2 are quartic centrifugal distortion constants. χ_{aa}, χ_{bb}, and χ_{cc} are ^{14}N nuclear quadrupole coupling constants. V_3 is the internal rotation barrier. D_{pi2J} is an empirical internal rotation-overall rotation distortion parameter.[76] δ is the angle of the internal rotation axis with the a inertial axis. ε is the angle between the principal inertial axis b and the projection of the internal rotation axis onto the bc plane. N is the number of hyperfine quadrupole components fitted. σ is the standard deviation of the fit. I_α is the moment of inertia of methyl top. F is the methyl top internal rotational reduced constant, $F = F/r$ ($r = 1-\Sigma_g(\lambda_g^2 I_\alpha/I_g)$; $g = a, b, c$; $\lambda_g= \cos(\angle(i,g))$. $\angle(i,a)$, $\angle(i,b)$, $\angle(i,c)$ are the angles between the methyl top axis and the inertial axes a, b and c ($\delta=\angle(i,a)$). [b] Standard errors are given in parentheses in units of the last digits. [c] Parameters in square brackets were kept fixed. I_α was assumed to have the same value given for 2-butanone.[46] Starting values for the geometrical parameters were taken from the CCSD/6-311++G(2d,p) optimized geometry.

The first assignments of the rotational spectrum of the *AA* sub-state of the complex PY···ACE were done using a semirigid Hamiltonian but the analysis of the full set of *AA*, *AE*, *EA*, and *EE* torsion substates was finally done using the XIAM program. The results are collected in Table 2 and the observed frequencies in Table S12.

Table 2. Rotational parameters obtained from the internal rotation analysis of the pyridine···acetone spectrum and their comparison to those calculated at CCSD/6-311++G(2d,p) level. The centrifugal distortion constants and the V_3 barrier have been calculated at MP2/6-311++G(2d,p).

Param [a]	Obs	Calc
A/MHz	2722.6132(14)[b]	2722.8
B/MHz	627.32262(26)	630.4
C/MHz	575.35393(23)	577.3
D_J/kHz	0.2308(31)	0.22
D_{JK}/kHz	2.104(48)	1.76
D_K/kHz	[0.0]	-1.75
d_1/kHz	[0.0]	-0.017
d_2/kHz	-0.0106(41)	0.015
χ_{aa}/MHz	-4.1446(86)	-4.47
$(\chi_{bb}-\chi_{cc})$ /MHz	-2.4688(96)	-2.59
V_3/GHz	7807.3(14)	7183
V_3/cm^{-1}	260.424(47)	239.6
V_3/kJmol^{-1}	3.11537(56)	2.866
D_{c3J}/kHz	-1.247(27)	
ε/rad	±2.0968(10)[d]	±2.12
δ/rad	1.63341(38)	1.65
I_α/uÅ^2	[3.215][c]	3.201
F/GHz	[157.1936][c]	158.488
$\angle(i,a)$/°	93.587(22)	94.5
$\angle(i,b)$/°	120.071(58)	121.4
$\angle(i_1,c)$/° [d]	30.329(59)	31.8
$\angle(i_2,c)$/° [d]	149.671(59)	148.2
N	182	
σ/kHz	7.2	

[a] A, B, and C are rotational constants. D_J, D_{JK}, D_K, d_1, and d_2 are quartic centrifugal distortion constants. χ_{aa}, $\chi_{bb,}$ and χ_{cc} are ^{14}N nuclear quadrupole coupling constants. V_3 is the internal rotation barrier. D_{c3J} is an empirical internal rotation-overall rotation distortion parameter.[76] δ is the angle of the internal rotation axis with the a inertial axis. ε is the angle between the principal inertial axis b and the projection of the internal rotation axis onto the bc plane. N is the number of hyperfine quadrupole components fitted. σ is the standard deviation of the fit. I_α is the moment of inertia of methyl top. F is the methyl top internal rotational reduced constant, $F = F/r$ ($r = 1-\Sigma_g(\lambda_g^2 I_\alpha/I_g)$; $g = a, b, c$; $\lambda_g= \cos(\angle(i,g))$. $\angle(i,a)$, $\angle(i,b)$, $\angle(i,c)$ are the angles between the methyl top axis and the inertial axes a, b, and c ($\delta=\angle(i,a)$) ; I_α was assumed to have the same value given for acetone.[44] Starting values for the geometrical parameters were taken from the CCSD/6-311++G(2d,p) optimized geometry. [d] The complex has two equivalent tops which share common values for all the parameters except for angles ε and $\angle(i,b)$/°.

Structural Considerations

Unfortunately, the intensities of the observed spectra did not allow the observation of ^{13}C isotopologues in their natural abundances to gain experimental information on the structures of the complexes. With the reduced set of experimental data, we cannot do a determination of the complex structures so we have taken the CCSD/6-311++G(2d,p) structures given in Tables S7-S8 as reasonably accurate descriptions. The geometrical parameters relevant to the intermolecular interactions are given in Figure 6. These parameters are compared in Table 3 and in Figure S3 with those of the previously studied complexes PY···FA[31] and PY···AC.[32] The spectroscopic parameters predicted

ARTICLE   **Journal Name**

from these structures are compared in Tables 1 and 2 with those experimentally determined. Experimental rotational constants are an excellent benchmark to test the structural data predicted from theory and in this case, are reproduced very well at this level of theory. A comparison between the calculated parameters and other DFT or MP2 methods can be seen in Tables S1, S2, S4, and S5, which do not show the same level of agreement. Similar results were found for the complexes PY···FA[31] and PY···AC[32] indicating CCSD/6-311++G(2d,p) level gives a reasonable description of the structure and nature of the interactions responsible for the formation of PY···2BU and PY···ACE complexes (see Tables S8 and S9). In the same way and as it was observed for PY···AC[32] we have also a good agreement between the CCSD and experimental internal rotation parameters, especially the angles $\angle(i,a)$, $\angle(i,b)$, $\angle(i,c)$, giving the orientation of the methyl top axis relative to the principal inertial axes (see Figure 6).

Methyl Group Internal Rotation

The analysis of the rotational spectra has allowed the determination of the barrier to internal rotation of the methyl groups in both complexes. In PY···ACE there are two equivalent methyl groups while in PY···2BU only the internal rotation barrier of the methyl group bonded to the C=O group has been determined from the observed *A-E* splittings. Splitting arising from the ethylic methyl group has not been observed within the resolution of the spectrometer used. The methyl internal rotation barriers determined for PY···AC,[32] PY···ACE, and PY···2BU are compared in Table 4 with those of the free AC,[77] ACE[44], or 2BU.[46] For the isolated monomers the barrier to internal rotation of the methyl group decreases from AC to ACE and finally 2BU. However, the effect of the formation of the complex on the barrier is remarkable. Decreases of *ca.* 64.0 cm^{-1} for AC and 5.7 cm^{-1} for ACE while an increment of *ca.* 34 cm^{-1} is observed for 2BU. The calculated methyl group internal rotation barriers at the MP2 level reproduced the experimental results showing a good correlation coefficient, $R^2 = 0.98$. It should be indicated that isolated ACE shows similar barriers as in the complex with PY. The experimental results indicate that the barrier is 6 cm^{-1} smaller in the complex while the calculations predicts that the barrier is larger by 11 cm^{-1} in the complex.

The decrease of the barrier height in PY···AC was shown to be related to the modulation of the $n \rightarrow \pi^*$ bond distance by the internal rotation motion.[32] In the PY···ACE and PY···2BU complexes analyzing the origin of the alterations of the internal rotation barriers is not straightforward. This would require a detailed analysis of the potential energy profile and the changes in the molecular, in particular, the r(N···C) Bürgi-Dunitz distance, along the minimum energy path for the methyl torsion coordinate. In both complexes, internal rotation is a two-dimensional problem although for PY···2BU the coordinates can be approximately separated. The two-dimensional potential energy function calculated at the MP2/6-311++G(2d,p) level for PY···ACE is shown in Figure S4 along with the one-dimensional profile which shows alterations in the phase and the shape

around the minima due to the intermolecular interactions. Similar behavior is predicted for PY···2BU at the same level. As shown in Figure S5, in both cases the periodical functions resulting from the difference between the one-dimensional profiles for the free and the bonded ketones show interesting phase relations with the predicted r(N···C) Bürgi-Dunitz distance oscillating profiles. The Bürgi-Dunitz distance is related to the $n \rightarrow \pi^*$ interaction energy,[31] so these predicted phase relationships suggest this intermolecular interaction is playing an important role in the alteration of the internal rotation energy profiles and barriers upon complexation with PY.

Table 3. Comparison of the experimental (r_0) and theoretical (r_e, CCSD/6-311++G(2d,p)) geometrical parameters describing the $n \rightarrow \pi^*$ tetrel bond interaction and the weak C-H···O=C HB for the series of complexes formed by pyridine (PY) with formaldehyde (FA), acetaldehyde (AC), acetone (ACE) and 2-butanone(2BU). The calculated dissociation energies (D_e) are listed in the last row.

	PY-FA[a]		PY-AC[b]		PY·ACE	PY-2BU
	r_0	r_e	r_0	r_e	r_e	r_e
r(N···C) /Å	2.855(4)	2.865	3.012(2)	3.012	3.118	3.095
$\angle$N···C=O/°	102.8(6)	102.5	96.9(2)	96.7	92.6	91.7
$\angle C_4$·N···C/°	156.5(8)	157.0	154.27(8)	154.7	153.3	152.2
r(O···H)/Å	2.53(2)	2.534	2.474(3)	2.478	2.439	2.435
$\angle$C=O···H/°	94.7(6)	94.8	99.8(1)	99.7	103.5	104.5
D_e^c/kJ mol^{-1}	15.9		15.9		17.2	19.0

[a] Taken from reference 31; [b] Taken from reference 32; Data for PY-ACE and PY-2BU taken from this work; [c] The dissociation energy, D_e, has been obtained at CCSD(T)/6-311++G(2d,p)//CCSD/6-311++G(2d,p) computational level including the BSSE correction.

	PY-AC[a]	AC[b]	PY-ACE[c]	ACE[d]	PY-2BU[c]	2-BU[e]
Exp.	343.6	407.5977	260.42	266.10	220.98	183.170
MP2	348.4	396.0	239.6	228.3	197.7	160.0

[a] Taken from reference 32; [b] Taken from reference 77; [c] This work; [d] Taken from reference 44 ; [e] Taken from reference 46.
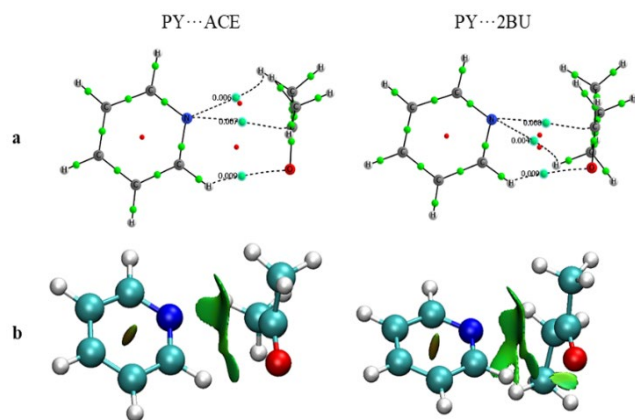

Figure 7. AIM and NCIPlot figures of the most stable minima for pyridine···acetone (PY···ACE) and pyridine···2-butanone (PY···2BU). The ρ values (au) in the intermolecular BCPs are indicated.

Nature of the intermolecular interactions

The theoretical structures of the complexes PY···ACE and PY···2BU are consistent with their formation through an $n{\rightarrow}\pi^*$ interaction. The experimental rotational constants and the geometrical parameters derived from the internal rotation
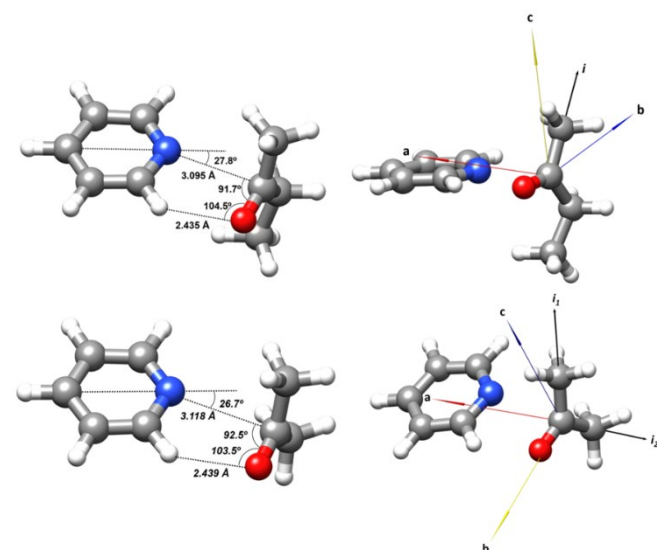

Figure 6. CCDS/6-311++G(2d,p) geometrical parameters. In the figures on the right the principal inertial axes have been translated to the carbonyl C atom and show the i CH$_3$ top axes allowing to envisage the definition of the angles $\angle(i,a)$, $\angle(i,b)$, and $\angle(i,c)$, determined from the internal rotation analysis of the spectra given in Tables 1 and 2.

analysis (see Tables 1 and 2) are in excellent agreement with the

CCSD predictions so they can be taken as good descriptions of the structures of the complexes. Two of the signatures of the $n{\rightarrow}\pi^*$ interactions are evident from these structures. The N atom is in the plane bisecting the HCH angle (C_s symmetry). The r(N···C) distances are 3.089(3) Å for PY···2BU and 3.126(2) Å for PY···ACE, both of them shorter than the sum of van der Waals radii, 3.25 Å. The Bürgi–Dunitz angle $\angle$N···C=O values are 92.3(7)° and 91.7(2)°, out of the predicted range of 107° ± 10°, but not far from it. A comparison of these parameters with those of PY···FA (r(N···C) = 2.855(3) Å, $\angle$N···C=O = 102.8(6)°) or PY···AC (r(N···C) = 3.012(3) Å, $\angle$N···C=O = 96.9(2)°) indicates that the interaction weakens throughout the series FA→AC→ACE≈2BU, so that PY···FA could be taken as the best reference to characterize this kind of $n{\rightarrow}\pi^*$ tetrel interaction. On the other hand, the parameters related to the weak hydrogen contact C-H···O=C reflect the reverse behavior if we consider the H···C distance, which progressively decreases from PY···FA to PY···2BU, and the $\angle$C=O···H angle, which despite being far from a linear arrangement of the bond increases throughout the series from PY···FA to PY···2BU. Table 3 also includes dissociation energies calculated at CCSD(T)/6-311++G(2d,p)//CCSD/6-311++G(2d,p) computational level including the BSSE correction. The dissociation energy of the complexes is similar for the two smallest complexes (15.9 kJ mol^{-1}) while for the two largest, it increases with the size of the carbonyl derivatives up to 19.0 kJ mol^{-1} in PY···2BU. These data also suggest a delicate interplay between both the $n{\rightarrow}\pi^*$ and weak HBs in these systems under the influence of other weak steric N···C and N···O interactions between PY, the C=O group and its substituents. The influence of the interaction between PY and the methyl group of AC on the $n{\rightarrow}\pi^*$ bond distance was found to be responsible for the notable decrease in the barrier to internal rotation of the methyl group in PY···AC with respect to free AC.[32]

The components of the SAPT analysis are gathered in Table 5. The binding energy is dominated by the electrostatic and dispersion terms. The electrostatic one is the most important for the PY···FA (52% of the attractive term) but decreases as the size of the carbonyl derivative increases, being 45 % of all the attractive terms in PY···2BU. On the contrary, the dispersion increases with the size of the carbonyl derivative from 33 % to 45%. In fact, for the PY···2BU complex, the electrostatic and the dispersion terms have the same contribution.

Table 5. SAPT terms (kJ mol^{-1}) calculated in this work for the different pyridine(PY)···RR'C=O observed. R=R'=H, formaldehyde (FA); R=H, R'=CH$_3$, acetaldehyde (AC); R=R'=CH$_3$, acetone; R= CH$_3$, R'=CH$_2$CH$_3$, 2-butanone (2BU).

Complex	Elect.	Exch.	Ind.	Disp.	δHF	E$_{SAPT}$
PY···FA	-24.9	30.2	-3.2	-16.0	-3.9	-17.9
PY···AC	-22.3	27.5	-3.0	-17.6	-2.5	-17.8
PY···ACE	-22.3	28.5	-3.2	-20.2	-2.1	-19.4
PY···2BU	-24.0	32.2	-3.4	-24.0	-2.3	-21.3

In Figure 7, the results of the AIM (a) and NCIPlot (b) analyses of the observed conformers of PY···ACE and PY···2BU are depicted. The graphs show the $n \rightarrow \pi^*$ and weak CH···O HB. In addition, a weak N···HC interaction is observed. All the intermolecular bond critical points show the typical signature of weak interaction (small values of ρ, between 0.011 and 0.007 au, and positive Laplacian). The values ρ at the intermolecular BCPs (N···C and O···H contacts) follow exponential relationships with the distance, in agreement with previous reports on HB and other NCIs (see Table S10 and Figure S6).[78,79]
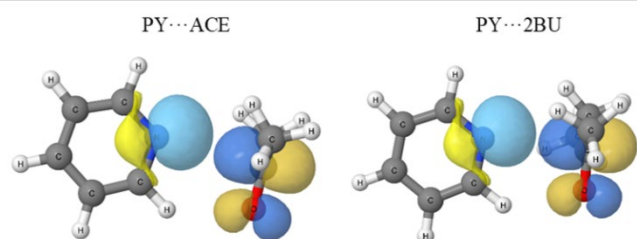

Figure 8. Orbitals involved in the charge transfer between N(lp) and π* CO.

Table 6.- Results of the NBO analysis of the most important charge transfer in the complexes pyridine(PY)···RR'C=O; R=R'=H, formaldehyde (FA); R=H, R'=CH$_3$, acetaldehyde (AC); R=R'=CH$_3$, acetone; R= CH$_3$, R'=CH$_2$CH$_3$, 2-butanone (2BU).

	PY-FA[a]	PY-AC[b]	PY-ACE[c]	PY-2BU[c]
r(N···C) /Å	2.865	3.012	3.118	3.095
N(lp) → π* CO	14.4	7.6	4.9	5.6
r(O···H) /Å	2.534	2.478	2.439	2.435
O(lp) → σ* CH	0.8	1.0	1.2	1.3

[a] Taken from reference 31. [b] Taken from reference 32. [c] This work

Based on the NBO analysis the most important stabilizing charge transfer between occupied orbitals of one molecule and empty ones of the other molecule corresponds to the N(lp)→π* CO (Figure 8). They account for 4.9 and 5.6 kJ mol^{-1} in the complexes of PY with ACE and 2BU, respectively (Table 6). These values are smaller than in the PY···FA and PY···AC complexes (14.4 and 7.6 kJ mol^{-1}, respectively). A clear relationship is found between the N(lp)→π* CO stabilization energy and the intermolecular N-C, which shorter distances imply stronger stabilizations.

The contribution of the CH···O HB (O(lp)→σ* CH) is much smaller than the tetrel bond, between 0.8 to 1.3 kJ mol^{-1}. In this case, the stabilization contribution of this interaction increases with the size of the carbonyl group being the smallest in the PY···FA complex (0.8 kJ mol^{-1}) and the largest in the PY···2BU (1.3 kJ mol^{-1}).

Conclusions

In this work, we have presented the results of a combined theoretical and experimental study of the complexes of PY with two of the simplest ketones, ACE, and 2BU. In both cases, the main intermolecular interaction is an $n \rightarrow \pi^*$ tetrel interaction from the PY nitrogen to the carbonyl carbon atom of the ketone, involving the nitrogen atom lone pair and the antibonding π^* C=O orbital. This interaction is reinforced by a weak C-H···O HB

involving one of the PY C-H groups adjacent to the N atom and the carbonyl oxygen atom. The same interactions were observed previously in the related complexes of PY with FA[31] and AC.[32] As previously observed,[31,32] CCSD/6-311++G(2d,p) calculations give very good predictions of the rotational constants, so the geometries predicted at this level of theory can be considered as reasonable estimations close to the experimental ones. A comparison of the structures and bond properties of the complete series of PY complexes with FA, AC, ACE, and 2BU, indicates that the $n \rightarrow \pi^*$ tetrel interaction energy decreases along with the series FA>AC>2BU≈ACE. This decrease in energy could be related to the size of the PY partner and to the increase in the steric interactions of the carbonyl substituents with PY. These interactions force the carbonyl carbon to move away from nitrogen. At the same time, the C-H···O HB seems to be not so hampered since the steric repulsions mainly affect the N atom and its strength increases reversely, FA<AC<2BU≈ACE as the $n \rightarrow \pi^*$ tetrel interaction weakens. This C-H···O interaction also forces the Bürgi-Dunitz angle ∠N···C=O to be out of the predicted optimum interval in the ketone complexes, probably another additional contribution to weakening the tetrel bond. Thus, the interaction of PY with aldehydes or ketones is governed by an intricate balance of attractive interactions, such as $n \rightarrow \pi^*$ and C-H···O, together with the effects of the internal rotation dynamics and repulsive steric forces, which increase with the ketone size making the complexes presumably less stable than the complexes PY···FA or PY···AC. The DFT-SAPT analysis shows how the electrostatic term is dominant in the PY···FA, decreasing with the size of the carbonyl molecule, while the dispersion increases with the size of this moiety. Thus, In the PY···2BU complex, electrostatic and dispersion have similar stabilizing contributions.

Another interesting fact observed in this work concerns to the internal rotation of the methyl groups in ACE and 2BU. We have shown that the V_3 internal rotation barrier of free AC decreases by 64 cm^{-1} upon formation of the PY···AC complex.[32] The analysis of the internal rotation splittings in the PY···ACE and PY···2BU rotational spectra has allowed the determination of the V_3 barriers in those complexes. Upon complexation, the barrier slightly decreases by 5.7 cm^{-1} for ACE, but increases by 34 cm^{-1} for 2BU. As was shown for PY···AC,[32] the theoretical calculations on PY···ACE and PY···2BU suggest that the geared oscillation of the Bürgi-Dunitz interaction parameters, like the r(N···C) distance related to the intermolecular interaction strength, may play an important role in modifying the internal rotation energy profiles in the complexes.

Conflicts of interest

There are no conflicts to declare".

Acknowledgments

Notes and references

1   J. M. Lehn, Supramolecular Chemistry—Scope and Perspectives Molecules, Supermolecules, and Molecular Devices (Nobel Lecture), *Angew. Chem. Int. Ed.*, 1988, **27**, 89–112.

2   J. M. Lehn, Toward self-organization and complex matter, *Science*, 2002, **295**, 2400–2403.

3   C. Desfrançois, S. Carles and J. P. Schermann, Weakly bound clusters of biological interest, *Chem. Rev.*, 2000, **100**, 3943–3962.

4   M. T. Doppert, H. van Overeem and T. J. Mooibroek, Intermolecular π-hole/n→π* interactions with carbon monoxide ligands in crystal structures, *Chem. Commun.*, 2018, **54**, 12049–12052.

5   J. Echeverría, The n → π* interaction in metal complexes, *Chem. Commun.*, 2018, **54**, 3061–3064.

6   F. Weinhold and C. R. Landis, *Valency and Bonding*, Cambridge University Press, Cambridge, 2005.

7   R. S. Mulliken, Structures of Complexes Formed by Halogen Molecules with Aromatic and with Oxygenated Solvents, *J. Am. Chem. Soc.*, 1950, **72**, 600–608.

8   G. Cavallo, P. Metrangolo, R. Milani, T. Pilati, A. Priimagi, G. Resnati and G. Terraneo, The halogen bond, *Chem. Rev.*, 2015, **116**, 2478–2601.

9   I. Alkorta, J. Elguero and A. Frontera, Not only hydrogen bonds: Other noncovalent interactions, *Crystals*, 2020, **10**, 180.

10   A. Bauzá, T. J. Mooibroek and A. Frontera, Tetrel-Bonding Interaction: Rediscovered Supramolecular Force?, *Angew. Chem. Int. Ed.*, 2013, **52**, 12317–12321.

11   I. Alkorta, I. Rozas and J. Elguero, Molecular Complexes between Silicon Derivatives and Electron-Rich Groups, *J. Phys. Chem. A*, 2001, **105**, 743–749.

12   S. J. Grabowski, Tetrel bond-σ-hole bond as a preliminary stage of the SN2 reaction, *Phys. Chem. Chem. Phys.*, 2014, **16**, 1824–1834.

13   S. Scheiner, A new noncovalent force: Comparison of P...N interaction with hydrogen and halogen bonds, *J. Chem. Phys.*, 2011, **134**, 94315.

14   S. Zahn, R. Frank, E. Hey-Hawkins and B. Kirchner, Pnicogen bonds: A new molecular linker?, *Chem. Eur. J.*, 2011, **17**, 6034–6038.

15   J. E. Del Bene, I. Alkorta, G. Sanchez-Sanz and J. Elguero, Structures, binding energies, and spin-spin coupling constants of geometric isomers of pnicogen homodimers (PHFX) 2, X = F, Cl, CN, CH 3, NC, *J. Phys. Chem. A*, 2012, **116**, 3056–3060.

16   W. Wang, B. Ji and Y. Zhang, Chalcogen bond: A sister noncovalent bond to halogen bond, *J. Phys. Chem. A*, 2009, **113**, 8132–8135.

17   R. M. Minyaev and V. I. Minkin, Theoretical study of O - > X (S, Se, Te) coordination in organic compounds, *Can. J. Chem.*, 2011, **76**, 776–788.

18   G. Sánchez-Sanz, C. Trujillo, I. Alkorta and J. Elguero, Intermolecular Weak Interactions in HTeXH Dimers (X=O, S, Se, Te): Hydrogen Bonds, Chalcogen–Chalcogen Contacts and Chiral Discrimination, *ChemPhysChem*, 2012, **13**, 496–503.

19   I. Alkorta and A. Legon, An Ab Initio Investigation of the Geometries and Binding Strengths of Tetrel-, Pnictogen-, and Chalcogen-Bonded Complexes of CO2, N2O, and CS2 with Simple Lewis Bases: Some Generalizations, *Molecules*, 2018, **23**, 2250.

20   A. C. Legon, Tetrel, pnictogen and chalcogen bonds identified in the gas phase before they had names: A systematic look at non-covalent interactions, *Phys. Chem. Chem. Phys.*, 2017, **19**, 14884–14896.

21   G. Cavallo, P. Metrangolo, T. Pilati, G. Resnati and G. Terraneo, Naming interactions from the electrophilic site, *Cryst. Growth Des.*, 2014, **14**, 2697–2702.

22   R. W. Newberry and R. T. Raines, The n →π* Interaction, *Acc. Chem. Res.*, 2017, **50**, 1838–1846.

23   R. Paulini, K. Müller and F. Diederich, Orthogonal multipolar interactions in structural chemistry and biology, *Angew. Chem. Int. Ed.*, 2005, **44**, 1788–1805.

24   S. Blanco, J. C. López, S. Mata and J. L. Alonso, Conformations of γ-aminobutyric acid (gaba): The role of the n→π* interaction, *Angew. Chem. Int. Ed.*, 2010, **49**, 9187–9192.

25   A. Lesarri, E. J. Cocinero, J. C. López and J. L. Alonso, Shape of 4(S)- and 4(R)-hydroxyproline in gas phase, *J. Am. Chem. Soc.*, 2005, **127**, 2572–2579.

26   M. E. Sanz, A. Lesarri, M. I. Peña, V. Vaquero, V. Cortijo, J. C. López and J. L. Alonso, The shape of β-alanine, *J. Am. Chem. Soc.*, 2006, **128**, 3812–3817.

27   R. G. Bird, V. Vaquero-Vara, D. P. Zaleski, B. H. Pate and D. W. Pratt, Chirped-pulsed FTMW spectra of valeric acid, 5-aminovaleric acid, and γ-valerolactam: A study of amino acid mimics in the gas phase, *J. Mol. Spectrosc.*, 2012, **280**, 42–46.

28   C. Cabezas, J. L. Alonso, J. C. López and S. Mata, Unveiling the Shape of Aspirin in the Gas Phase, *Angew. Chem. Int. Ed.*, 2012, **51**, 1375–1378.

29   G. J. Bartlett, A. Choudhary, R. T. Raines and D. N. Woolfson, n→π* interactions in proteins, *Nat. Chem. Biol.*, 2010, **6**, 615–620.

30   L. E. Bretscher, C. L. Jenkins, K. M. Taylor, M. L. DeRider and R. T. Raines, Conformational stability of collagen relies on a stereoelectronic effect, *J. Am. Chem. Soc.*, 2001, **123**, 777–778.

31   S. Blanco and J. C. López, Rotational Characterization of an n → π∗ Interaction in a Pyridine-Formaldehyde Adduct, *J. Phys. Chem. Lett.*, 2018, **9**, 4632–4637.

32   S. Blanco, A. Macario and J. C. López, Pyridine–acetaldehyde, a molecular balance to explore the n→π* interaction, *Phys. Chem. Chem. Phys.*, 2019, **21**, 20566–20570.

33   J. Chen, H. Wang, Z. Kisiel, Q. Gou and W. Caminati, Hydrogen versus tetrel bonds in complexes of 3-oxetanone with water and formaldehyde, *Phys. Chem. Chem. Phys.*, 2021, **23**, 7295–7301.

34   C. Pérez, J. L. Neill, M. T. Muckle, D. P. Zaleski, I. Peña, J. C. López, J. L. Alonso and B. H. Pate, Water-Water and Water-Solute Interactions in Microsolvated Organic Complexes, *Angew. Chem. Int. Ed.*, 2015, **54**, 979–982.

35   H. Bürgi, J. Dunitz and E. Shefter, Geometrical reaction coordinates. II. Nucleophilic addition to a carbonyl group, *J. Am. Chem. Soc.*, 1973, **587**, 5065–5067.

36   H. B. Bürgi, J. D. Dunitz, J. M. Lehn and G. Wipff, Stereochemistry of reaction paths at carbonyl centres, *Tetrahedron*, 1974, **30**, 1563–1572.

37   H. B. Bürgi, J. D. Dunitz, E. Shefter and IUCr, Chemical reaction paths. IV. Aspects of O.C = O interactions in crystals, *Acta Crystallogr. Sect. B*, 1974, **30**, 1517–1527.

38   M. L. DeRider, S. J. Wilkens, M. J. Waddell, L. E. Bretscher, F. Weinhold, R. T. Raines and J. L. Markley, Collagen stability: Insights from NMR spectroscopic and hybrid density functional computational investigations of the effect of electronegative substituents on prolyl ring conformations, *J. Am. Chem. Soc.*, 2002, **124**, 2497–2505.

39   M. P. Hinderaker and R. T. Raines, An electronic effect on protein structure., *Protein Sci.*, 2003, **12**, 1188–1194.

40   A. Choudhary, K. J. Kamer and R. T. Raines, An n→π* interaction in aspirin: implications for structure and reactivity., *J. Org. Chem.*, 2011, **76**, 7933–7937.

41   W. Li, M. M. Quesada-Moreno, P. Pinacho and M. Schnell, Unlocking the Water Trimer Loop: Isotopic Study of Benzophenone-(H_2O) $_{1-3}$ Clusters with Rotational Spectroscopy, *Angew. Chem. Int. Ed.*, 2021, **60**, 5323–5330.

42   R. Tandon, T. Unzner, T. A. Nigst, N. De Rycke, P. Mayer, B. Wendt, O. R. P. David and H. Zipse, Annelated Pyridines as Highly Nucleophilic and Lewis Basic Catalysts for Acylation Reactions, *Chem. Eur. J.*, 2013, **19**, 6435–6442.

43   P. M. J. Szell, S. Zablotny and D. L. Bryce, Halogen bonding as a supramolecular dynamics catalyst, *Nat. Commun.*, 2019, **10**, 916.

44   J. M. Vacherand, B. P. Van Eijck, J. Burie and J. Demaison, The rotational spectrum of acetone: Internal rotation and centrifugal distortion analysis, *J. Mol. Spectrosc.*, 1986, **118**, 355–362.

45   L. Pierce, C. K. Chang, M. Hayashi and R. Nelson, Microwave spectrum, dipole moment, and internal rotation of trans-2-butanone, *J. Mol. Spectrosc.*, 1969, **32**, 449–457.

46   H. V. L. Nguyen, V. Van, W. Stahl and I. Kleiner, The effects of two internal rotations in the microwave spectrum of ethyl methyl ketone, *J. Chem. Phys.*, 2014, **140**, 214303.

47   G. G. Brown, B. C. Dian, K. O. Douglass, S. M. Geyer, S. T. Shipman and B. H. Pate, A broadband Fourier transform microwave spectrometer based on chirped pulse excitation, *Rev. Sci. Instrum.*, 2008, **79**, 4–5.

48   P. Pinacho, S. Blanco and J. C. López, The complete conformational panorama of formanilide–water complexes: the role of water as a conformational switch, *Phys. Chem. Chem. Phys.*, 2019, **21**, 2177–2185.

49   Z. Kisiel, Assignment and Analysis of Complex Rotational Spectra, *Spectrosc. from Sp.*, 2001, 91–106.

50   Z. Kisiel, PROSPE. Programs for Rotational Spectroscopy, http://www.ifpan.edu.pl/~kisiel/prospe.htm.

51   P. Pracht, F. Bohle and S. Grimme, Automated exploration of the low-energy chemical space with fast quantum chemical methods, *Phys. Chem. Chem. Phys.*, 2020, **22**, 7169–7192.

52   A. D. Becke, Density-functional thermochemistry.III. The role of exact exchange, *J. Chem. Phys.*, 1993, **98**, 5648.

53   C. Lee, W. Yang and R. G. Parr, Development of the Colle-Salvetti correlation-energy formula into a functional of the electron density, *Phys. Rev. B*, 1988, **37**, 785–789.

54   M. J. Frisch, J. A. Pople and J. S. Binkley, Self-consistent molecular orbital methods 25. Supplementary functions for Gaussian basis sets, *J. Chem. Phys.*, 1984, **80**, 3265–3269.

55   S. Grimme, S. Ehrlich and L. Goerigk, Effect of the damping function in dispersion corrected density functional theory, *J. Comput. Chem.*, 2011, **32**, 1456–1465.

56   C. Møller and M. S. Plesset, Note on an approximation treatment for many-electron systems, *Phys. Rev.*, 1934, **46**, 618–622.

57   M. J. Frisch et al, Gaussian 16, Revision A.03, *Gaussian Inc., Wallingford CT, 2016*.

58   S. F. Boys and F. Bernardi, The calculation of small molecular interactions by the differences of separate total energies. Some procedures with reduced errors, *Mol. Phys.*, 1970, **19**, 553–566.

59   H.-J. Werner, P. J. Knowles, G. Knizia, F. R. Manby and M. Schütz, Molpro: a general-purpose quantum chemistry program package, *WIREs Comput Mol Sci*, 2012, **2**, 242–253.

60   T. Lu and F. Chen, Multiwfn: A multifunctional wavefunction analyzer, *J. Comput. Chem.*, 2012, **33**, 580–592.

61   Jmol: an open-source Java viewer for chemical structures in 3D, http://www.jmol.org/.

62   G. Jansen, A. Hesselmann, H. L. Williams and C. F. Chabalowski, Comment on 'using Kohn-Sham orbitals in symmetry-adapted perturbation theory to investigate intermolecular interactions', *J. Phys. Chem. A*, 2001, **105**, 11156–11158.

63   C. Adamo and V. Barone, Toward reliable density functional methods without adjustable parameters: The PBE0 model, *J. Chem. Phys.*, 1999, **110**, 6158–6170.

64   R. F. W. Bader, A quantum theory of molecular structure and its applications, *Chem. Rev.*, 1991, **91**, 893–928.

65   T. A. Keith, AIMAll (Version 19.10.12), *TK Gristmill Software, Overl. Park KS, USA (aim.tkgristmill.com), 2019*.

66   J. Contreras-García, E. R. Johnson, S. Keinan, R. Chaudret, J. P. Piquemal, D. N. Beratan and W. Yang, NCIPLOT: A program for plotting noncovalent interaction regions, *J. Chem. Theory Comput.*, 2011, **7**, 625–632.

67   E. D. Glendening, J. K. Badenhoop, A. E. Reed, J. E. Carpenter, J. A. Bohmann, C. M. Morales, P. Karafiloglou, C. R. Landis and F. Weinhold, NBO 7.0, *Theor. Chem. Institute,*

Univ. Wisconsin, Madison., 2018.

68   N. Heineking, H. Dreizler and R. Schwarz, Nitrogen and Deuterium Hyperfine Structure in the Rotational Spectra of Pyridine and [4-D] Pyridine., *Z. Naturforsch.*, 1986, **41a**, 1210–1213.

69   R. J. Myers and E. Bright Wilson, Application of symmetry principles to the rotation-internal torsion levels of molecules with two equivalent methyl groups, *J. Chem. Phys.*, 1960, **33**, 186–191.

70   H. Hartwig and H. Dreizler, The Microwave Spectrum of trans-2,3-Dimethyloxirane in Torsional Excited States, *Z. Naturforsch.*, 1996, **51a**, 923–932.

71   H. M. Pickett, The fitting and prediction of vibration-rotation spectra with spin interactions, *J. Mol. Spectrosc.*, 1991, **148**, 371–377.

72   J. K. G. Watson, in *Vibrational Spectra and Structure a Series of Advances, Vol 6*, ed. J. R. Durig, Elsevier, New York, 1977, pp. 1–89.

73   W. Gordy and R. L. Cook, *Microwave molecular spectra*, Wiley-Interscience, New York, 1984, vol. 11.

74   D. Gerhard, A. Hellweg, I. Merke, W. Stahl, M. Baudelet, D. Petitprez and G. Wlodarczak, Internal rotation and chlorine nuclear quadrupole coupling of o-chlorotoluene studied by microwave spectroscopy and ab initio calculations, *J. Mol. Spectrosc.*, 2003, **2852**, 234–241.

75   R. C. Woods, A general program for the calculation of internal rotation splittings in microwave spectroscopy. Part II. The n-top problem, *J. Mol. Spectrosc.*, 1967, **22**, 49–59.

76   N. Hansen, H. Mäder and T. Bruhn, A molecular beam Fourier transform microwave study of 0 -tolunitrile: 14 N nuclear quadrupole coupling and methyl internal rotation effects, *Mol. Phys.*, 1999, **97**, 587–595.

77   I. A. Smirnov, E. A. Alekseev, V. V. Ilyushin, L. Margulés, R. A. Motiyenko and B. J. Drouin, Spectroscopy of the ground, first and second excited torsional states of acetaldehyde from 0.05 to 1.6 THz, *J. Mol. Spectrosc.*, 2014, **295**, 44–50.

78   I. Mata, I. Alkorta, E. Molins and E. Espinosa, Universal features of the electron density distribution in hydrogen-bonding regions: A comprehensive study involving H···X (X=H, C, N, O, F, S, Cl, π) interactions, *Chem. Eur. J.*, 2010, **16**, 2442–2452.

79   G. Sánchez-Sanz, I. Alkorta and J. Elguero, Theoretical study of the HXYH dimers (X, Y = O, S, Se). Hydrogen bonding and chalcogen–chalcogen interactions, *Mol. Phys.*, 2011, **109**, 2543–2552.

TABLE OF CONTENTS ENTRY:

The main interactions between pyridine and small ketones are a N···C=O $n{\rightarrow}\pi^*$ tetrel bond and a C-H···O weak hydrogen bond as shown in this rotational study of the complexes pyridine···acetone and pyridine···2-butanone.